Nanoscale

Accepted Manuscript

This article can be cited before page numbers have been issued, to do this please use: H. Jia, D. Yang, X. Han, J. Cai, H. Liu and W. He, *Nanoscale*, 2016, DOI: 10.1039/C6NR00860G.

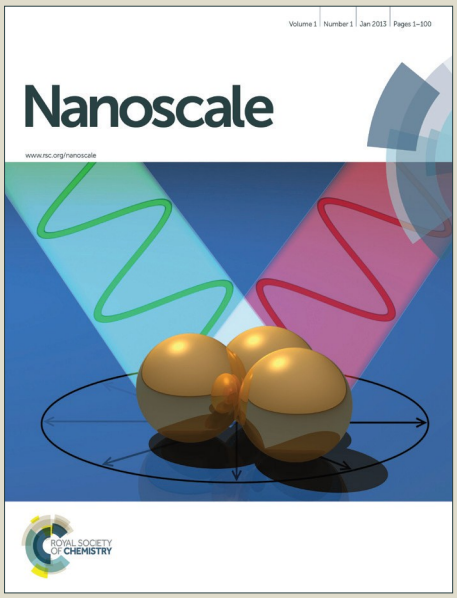

ROYAL SOCIETY OF CHEMISTRY

www.rsc.org/nanoscale

View Article Online
DOI: 10.1039/C6NR00860G

Journal Name

ARTICLE

Peroxidase-like Activity of Co_3O_4 Nanoparticles Used for Biodetection and Evaluation of Antioxidant Behavior †

Received 00th January 20xx,
Accepted 00th January 20xx

DOI: 10.1039/x0xx00000x

www.rsc.org/

Huimin Jia,[a] Dongfang Yang,[a] Xiangna Han,[a] Junhui Cai,[a] Haiying Liu[b] and Weiwei He*[a]

Nanostructured enzyme mimics are of great interest as promising alternatives to artificial enzymes for biomedical and catalytic applications. Studying the chemical interactions between antioxidants and nano-enzymes may yield a better understanding of the antioxidant capability of antioxidants and may help improve the function of artificial enzymes to better mimic natural enzymes. In this study, using Co_3O_4 nanoparticles (NPs) as peroxidase mimics to catalyze the oxidation of chromophoric substrates by H_2O_2, we developed a platform that acts as a biosensor for hydrogen peroxide and glucose and that can study the inhibitory effects of natural antioxidants on peroxidase mimics. This method can be applied specifically to glucose detection in real sample. Three natural antioxidants, gallic acid (GA), tannic acid (TA), and ascorbic acid (AA), were compared for their antioxidant capabilities. We found that these three antioxidants efficiently inhibit peroxidase-like activity with concentration dependence. The antioxidants exhibited different efficiencies, in the order of: tannic acid > gallic acid > ascorbic acid. They also showed distinct modes of inhibition based on different interaction mechanisms. This study served as a proof-of-concept that nano-enzyme mimics can be used to evaluate antioxidant capabilities and to screen enzymes inhibitors.

1. Introduction

Nanostructured artificial enzymes, a new class of enzyme mimics, have been the focus of much recent interest due to their robust catalytic activities and potential applications in biosensing, food processes, and environmental protection.[1,2] Since the discovery by Yan and coworkers that Fe_3O_4 NPs exhibit intrinsic peroxidase-like activity and have potential use in bioassays,[3] many scientists have explored the enzyme-like activity of nanomaterials. To date, a variety of inorganic nanomaterials, including metal oxides (Co_3O_4,[4] CeO_2,[5] V_2O_5,[6] CuO,[7] MnO_2[8]), metal sulfides (CuS, FeS),[9,10] noble metals (Au, Pt, Pd, AgM, Pd@Pt, Pd@Ir),[11-15] carbon (fullerene, graphene),[16,17] and metal organic frameworks [18] and their combined nanostructures (e.g. Fe_3O_4/Au, Pd/Fe_3O_4-PEI-RGO),[19,20] have demonstrated peroxidase-like, oxidase-like, catalase-like, or SOD-like properties. Because NPs are extremely small and have a large surface area per unit volume, they generally exhibit superior catalytic activity and intrinsic ability to generate or scavenge reactive oxygen species. These properties are likely responsible for the mechanism by which the NPs mimic the catalytic activity of natural enzymes. In addition, NPs have several advantages over natural enzymes, including facile and low-cost synthesis, tunable catalytic activity, and high stability under stringent conditions. Nanostructures with enzyme-like activities thus have been considered as promising alternatives to enzyme mimetics.

The enzyme-like activity of NPs has been exploited for a number of applications. Bio-detection is the foremost application of nanomaterials as artificial enzymes.[3-5,22,23] Nanomaterials with peroxidase-like activity have been employed for colorimetric measurement of hydrogen peroxide (H_2O_2). H_2O_2 plays important roles as a signaling molecule in the regulation of biological processes and is a main by-product of many oxidation reactions involving biological molecules catalyzed by natural enzymes.[21] Nanomaterials with peroxidase-like activity have also been employed in specific enzyme reactions or competitive reactions with H_2O_2 for the detection of biologically active molecules such as glucose,[11] cholesterol,[22] xanthine,[23] metal ions, [24] and enzyme inhibitors.[25] Additionally, using nanostructured peroxidase mimics such as Fe_3O_4,[3] CeO_2,[5] Au@Pt, [12] and Pd@Ir[14] in place of natural peroxidase (HRP), NP-based colorimetric enzyme-linked immunosorbent assays (ELISA) have been developed for antigen/antibody detection. Beyond biosensing applications, a few NPs with peroxidase-like properties were found to exhibit excellent catalytic activities toward the degradation of organic pollutants or biotoxins, and may therefore be utilized for environmental protection applications.[26-27] Altogether, there have been extensive studies on the intrinsic enzyme-like activities of dozens of nanomaterials. In light of these discoveries, there are still many potential applications to

[a] Key Laboratory of Micro-Nano Materials for Energy Storage and Conversion of Henan Province, Institute of Surface Micro and Nano Materials, Xuchang University, Xuchang, Henan 461000, P. R. China. E-mail: heweiweixcu@gmail.com; Tel: +86-374-2968783
[b] Food and Bioengineering College, Xuchang University, Xuchang, Henan 461000, P. R. China.

†Electronic Supplementary Information (ESI) available: [Figure S1, S2, S3, S4, S5 and S6]. See DOI: 10.1039/x0xx00000x

View Article Online
DOI: 10.1039/C6NR00860G

explore that exploit the enzyme-mimicking properties of known nanomaterials.

Antioxidants are a group of molecules that have reducing power: they participate in redox reactions by donating electrons or hydrogen atoms. Many antioxidants from plant metabolites, including ascorbic acid, thiols, and polyphenols,[28] perform critical biological functions to maintain oxidative stress levels in organisms. They protect the body against oxidative damage caused by overproduction of reactive oxygen species associated with degenerative illness. Because of this, various antioxidants have been used as conventional additives in food products, cosmetics, and dietary supplements. The function and dosage of antioxidants are generally directed by their antioxidant capabilities and antioxidative mechanisms. Therefore, definitive techniques for evaluating antioxidant behaviors are needed to guide the use of different antioxidants. Various strategies with high selectivity or sensitivity have been employed to detect antioxidants, including liquid chromatography,[29] spectroscopy,[30] electrochemical sensing,[31] photo-electrochemistry,[32] and NPs based approaches.[33-35] However, a simple and reliable method to estimate antioxidant capacity and mechanism is still needed to quickly screen antioxidants and regulate their usage in related products.

Recently, Yin and co-workers reported that the peroxidase- or oxidase-like activities of Pt NPs exert an inhibitory effect on antioxidants (ascorbic acid and catechol).[22,36-37] They found that Au@Pt nanostructures inhibited the ability of ascorbic acid to reduce the levels of reactive oxygen species. In addition, Wu's group found that reducing agents also exhibited different inhibiting effects on the oxidase-like activity of Au@Pt nanorods.[25] Motivated by the inhibitive interactions between antioxidants and the nano-peroxidase mimetics, we present a novel platform for colorimetric evaluation of the antioxidant capability and antioxidant behaviors of natural antioxidants. Co_3O_4 NPs were selected as a model nano-peroxidase mimic due to ease of preparation, good stability in aqueous medium, and well-established peroxidase-like activity. Gallic acid, tannic acid, and ascorbic acid, three antioxidants that are often found in foods and dietary supplements, were used to demonstrate the feasibility of the proposed technique. In addition, we performed quantitative glucose detection by using peroxidase-like activity of Co_3O_4 NPs.

2. Experimental

2.1. Chemical and Materials

Cobalt nitrate hexahydrate ($Co(NO_3)_2 \cdot 6H_2O$), hexamethylene tetramine (HMTA), hydrogen peroxide (H_2O_2), α-D-glucose, o-phenylenediamine (OPD), 3, 3', 5, 5'-tetramethylbenzidine (TMB), tannic acid (TA) and gallic acid (GA) were analytically purified and were purchased from Sinopharm Chemical Reagent Co., Ltd (Beijing, China). L-ascorbic acid (AA) and glucose oxidase (from Aspergillus niger, GOx) were commercially from Aladdin Industrial Co. (CA, USA). Other chemicals were at least analytical reagent grade and used as received. Milli-Q water (18 MΩ. cm) was used for all experimental preparations. All glassware and autoclave used in the following procedures were cleaned by aqua regia solution (HNO_3/HCl = 1:3 v/v).

2.2. Synthesis of Co3O4 NPs

Co_3O_4 NPs were synthesized through a hydrothermal method. Typically, 0.1 mmol $Co(NO_3)_2$ and 0.1 mmol HMTA were dissolved in 16 ml dimethyl fumarate (DMF) under magnetically stirring for 15 min. The mixture then was transferred into a 21 ml Teflon-lined stainless steel autoclave. This autoclave was sealed, heated at 140 ºC for 14 h, and then air-cooled to room temperature. Finally, the black precipitate was collected by centrifugation, washed 2 times with ethonal and 1 time with water, and then diluted into 1 ml with water for further use.

2.3. Characterization

The phase structure of synthesized Co_3O_4 NPs was characterized by X-ray diffraction (XRD, Bruker D8 Advance diffractometer) with monochromatized Cu K_α radiation (λ =1.5418 Å). The samples for XRD analysis were prepared by dropping 10 µl Co_3O_4 suspensions on a 0.5 cm× 0.5 cm silicon wafer and dried under 60 ºC, until an evident film formed by repeating this operation couple times. Transmission electron microscopy (TEM) images were captured on a FEI TECNAI G^2 F20 U-TWIN transmission electron microscope at an accelerating voltage of 200 kV (National center for nanoscience and technology of China). The samples for TEM analysis were prepared by adding 8µl Co_3O_4 suspensions (diluted by 10 times) onto standard holey carbon-coated copper grids, which were then air dried at room temperature. UV-vis absorption spectra were obtained using a Varian Cary 5000 spectrophotometer.

2.4. Apparent kinetic analysis

The reaction kinetics for the catalytic oxidation of TMB and OPD catalyzed by Co_3O_4 NPs were studied by recording the absorption spectra with selected time interval in scanning kinetics mode. Unless otherwise stated, the reaction was carried out at room temperature and recorded immediately after the aqueous solution containing desired concentrations of H_2O_2 and TMB (OPD) mixed with 20 µg/ml Co_3O_4 NPs in 3.0 mL water. The antioxidant capabilities of GA, TA and AA were evaluated by addition of 20 µg/ml Co_3O_4 NPs into the mixture containing 20 µl 20 mM TMB, 10µl 0.1 M H_2O_2 and antioxidant at varying concentrations in 3ml H_2O, then the reaction process was monitored with 1 min interval. For TMB and OPD as substrate, the apparent kinetic parameters were calculated based on the Michaelise-Menten equation:

$$1/v = (K_m/V_{max}) \times (1/[S]) + 1/V_{max}$$

where v is the reaction initial velocity, V_{max} is the maximal reaction velocity, [S] is the concentration of substrate and K_m is the Michaelis constant.

2.5. Glucose detection

View Article Online
DOI: 10.1039/C6NR00860G

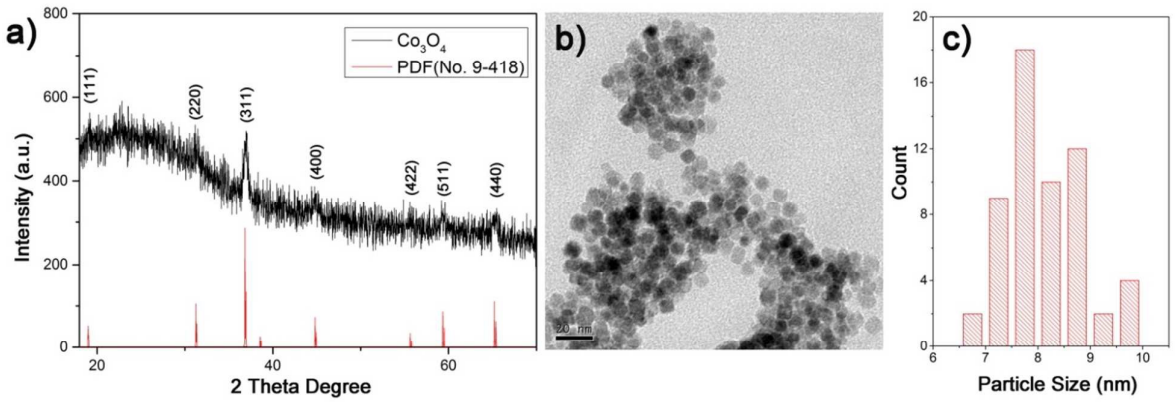

Figure 1. XRD pattern (a), TEM images (b), and size distributions (c) of as-prepared Co_3O_4 NPs.

Glucose was firstly oxidized catalyzed by glucose oxidase to produce gluconic acid and H_2O_2 in pH 7.4 buffer solution, and then the H_2O_2 was detected using TMB coloring reaction catalyzed by Co_3O_4. Glucose oxidase (20 μL, 100 Unit ml^{-1}) and glucose aqueous solution (480 μl) at varied concentrations were incubated at 37 ºC for 30 min. Then, 2.5 ml H_2O and 20 μl 20 mM TMB were added. Finally, 20 μl Co_3O_4 NPs was added to initiate the coloring reaction. The mixtures were incubated at 37 ºC for 30 min and then for UV-Vis spectra test. For selectivity analysis, maltose (1 mM), galactose (1 mM), and fructose (1 mM) were used instead of glucose. For testing the applicability of this method in real sample, the human blood serum from hospital was used as received and diluted by 100 fold. Standard addition method was used to detect the glucose in serum. Serum samples were spiked with 0, 0.033, 0.066 and 0.1 mM glucose, respectively. Then the unspiked and spiked serum samples were treated by same procedure as described above to set up the standard curve for detection of glucose.

3. Results and Discussion

3.1. Characterization of Co_3O_4 NPs

We used a simple method to prepare Co_3O_4 NPs by thermal treatment of Co^{2+} and hexamethylene tetramine (HMTA) in DMF at 140ºC for 12 h. The crystal structures and phase purities of the samples were first characterized by X-ray powder diffraction (XRD). The XRD pattern (**Figure 1a**) shows that all of the diffraction peaks can be indexed to the cubic phase of cobalt oxide (JCPDS No. 9-418) with the Fd-3m space group and a primitive cubic unit cell with a = 0.8084 nm. No other characteristic peaks of impurities were detected, indicating that the prepared Co_3O_4 NPs possessed good crystallinity. We then observed the morphology of Co_3O_4 NPs by TEM. As-prepared Co_3O_4 NPs typically displayed a quasi-cubic shape with good dispersibility (Figure 1b). The average diameter of the Co_3O_4 NPs was 8.3 ± 0.7 nm, as determined from measurement of 70 particles (Figure 1c). The Co_3O_4 NPs may possess superior catalytic properties due to their small particle size and the lack of additional surfactant modification.

3.2. Peroxidase-like activity of Co_3O_4 NPs

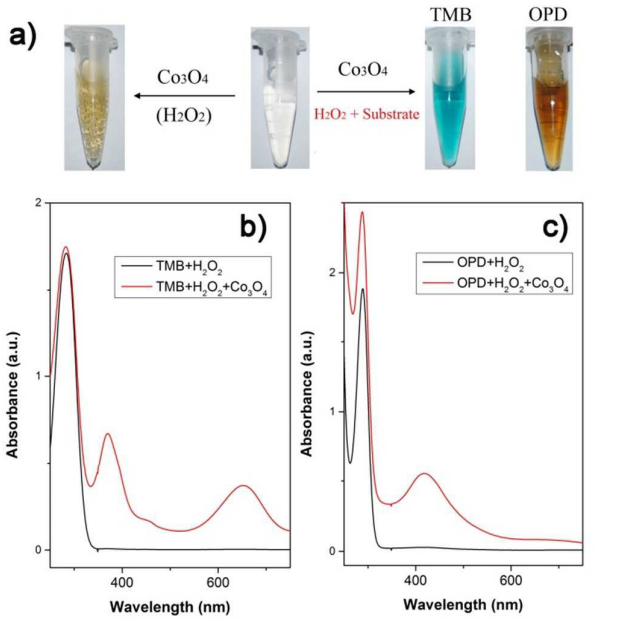

Figure 2 (a) The color evolution of TMB and OPD oxidation catalyzed by Co_3O_4 NPs in the presence of hydrogen peroxide (All the pictures were taken at 15 min after mixing), UV-VIS spectra obtained from samples containing 20 μl 0.1 mM H_2O_2 and 20 μl 20 mM TMB (b) or 20 μl 0.1 M OPD (c) in the absence and presence of Co_3O_4 NPs.

Table 1. Apparent kinetic parameters of Co_3O_4 for both TMB and OPD oxidation reactions. [Co_3O_4] is the Co_3O_4 particle concentration, [H_2O_2] is the concentration of hydrogen peroxide, K_m is the Michaelis constant, V_{max} is the maximal reaction velocity, and K_{cat} is the catalytic constant.

Substrate	[Co_3O_4](nM)	[H_2O_2](mM)	K_m (mM)	V_{max} (nM s^{-1})	K_{cat} [s^{-1}]
TMB	0.05	0.67	0.063	18.8	376
OPD	0.05	0.67	0.61	32.2	640

View Article Online
DOI: 10.1039/C6NR00860G

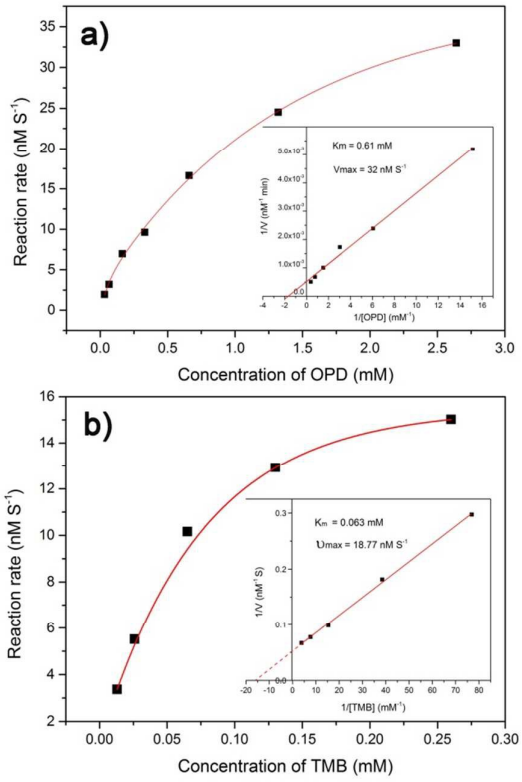

Figure 3 Effect of chromophoric substrate concentration on the reaction rate catalyzed by Co_3O_4 NPs. Reaction rates were found to be dependent on the concentrations of OPD (a) and TMB (b). Insets in panels (a) and (b) show the corresponding double-reciprocal plots for calculation of enzyme kinetic parameters by the Michaelis-Menten equation.

3, 3', 5, 5'-tetramethylbenzidine (TMB) and o-phenylenediamine (OPD) are two substrates commonly used for immunoassays and for the evaluation of NP peroxidase-like activity. We used TMB and OPD to verify the peroxidase-like activity of Co_3O_4 NPs. Co_3O_4 NPs can quickly catalyze the oxidation of TMB and OPD in the presence of H_2O_2 to produce characteristic blue- and yellow-colored products, respectively, in 20 min (Figure 2a). Control reactions, performed either in the absence of Co_3O_4 or in the absence of H_2O_2, showed negligible color changes in the same time period. This indicates that Co_3O_4 NPs exhibit a peroxidase-like activity similar to HRP. Co_3O_4 NPs also can catalyse the decomposition of H_2O_2 to produce dioxygen bubbles, suggestive of catalase-like activity. These results are consistent with previous reports.[4] UV-VIS spectral analysis also supported the observed color changes (Figure 2b and c). In the absence of Co_3O_4, the spectra of TMB and OPD remained unchanged. Upon the addition of Co_3O_4 NPs, new absorption peaks appeared at 650 nm and 373 nm for TMB and 416 nm for OPD, and the absorbance increased dramatically with time after the addition of Co_3O_4. We then calculated the initial reaction rates catalyzed by Co_3O_4 NPs by monitoring the absorbance increases at 650 nm for TMB and 416 nm for OPD. The catalytic reaction rate was found to be dependent on the concentration of Co_3O_4 NPs. For example, during the OPD oxidation reaction, the absorbance at 416 nm increased when more Co_3O_4 NPs were added (Figure S1). The reaction rate of OPD oxidation was semi-linearly proportional to the concentration of Co_3O_4 NPs from 3.2 μg/ml to 64 μg/ml.

3.3. Effects of substrate concentration on reaction rate

The effect of TMB and OPD concentration on their oxidation rate in the presence of 0.67 mM H_2O_2 was investigated (**Figure 3** and Figure S2). Graphs of the reaction rate as a function of substrate concentration show hyperbolic curves for both OPD and TMB. The reaction rates increased gradually with increasing TMB or OPD concentration until reaching a maximum rate, indicating saturation of the reactivity of Co_3O_4 NPs. We then performed steady-state kinetic analysis to determine the apparent enzyme kinetic parameters for both TMB and OPD oxidation catalyzed by Co_3O_4 NPs in the presence of H_2O_2. The oxidized products concentrations of TMB and OPD were calculated by the Lambert–Beer law using the values ε_{TMB} = 39000 $M^{-1}cm^{-1}$ (at 650nm) and ε_{OPD} = 16700 $M^{-1}cm^{-1}$ (at 416 nm). Typical double-reciprocal plots, 1/v vs. 1/[S] (**Figure 3** insets), were constructed and fitted to the *Michaelis-Menten* equation to calculate the catalytic parameters (Table 1). The *Michaelis* constants (K_m) of the Co_3O_4 NPs for TMB and OPD were determined to be 0.063 mM and 0.61 mM, respectively. The catalytic constants of Co_3O_4 NPs for TMB and OPD were calculated to be 376 s^{-1} and 644 s^{-1}, respectively.

In comparison with the natural enzyme HRP (K_m=0.49 mM) and other NPs with peroxidase-like activity, including Fe_3O_4 (K_m =0.098 mM),[3] FeS (K_m = 1.43),[10] CeO_2 (3.8 mM),[5] Fe_2O_3 (0.307 mM),[38] MnO_2 (0.31 mM),[8] and CuO (0.013 mM) structures,[7] the Co_3O_4 NPs have a relatively lower K_m value. K_m is an indicator of affinity between enzyme and substrate: a lower K_m value indicates a higher affinity. These results suggest that peroxidase-like Co_3O_4 NPs have relatively high affinity for TMB and OPD. It has been well recognized that mixed valence metal oxide or sulfide NPs exhibiting intrinsic peroxidase-like activity may be resulted from the Fenton or Fenton-like reactions with hydrogen peroxide.[3,7,9,10] Unlike the Fenton reaction mechanism, however, Co_3O_4 NPs may go through an electron transfer mechanism to exhibit peroxidase like activity due to the high redox potential of Co^{3+}/Co^{2+}.[4] Co^{3+}/Co^{2+} species, exposed concomitantly on the surface of Co_3O_4 NPs having a redox potential of about 1.27 V,[39] endow Co_3O_4 with oxidative potential. Co^{3+} can directly oxidize the substrate (e.g. TMB) to produce typical color, concomitantly Co^{3+} was reduced to Co^{2+}. Then, Co^{2+} was oxidized back to Co^{3+} by hydrogen peroxide meanwhile H_2O_2 was reduced to water by acceptance of two electrons. In the whole process, Co_3O_4 NPs acted as electron transfer mediator and facilitated the reaction between H_2O_2 and TMB.

3.4. Biosensing hydrogen peroxide and glucose based on the peroxidase-like activity of Co_3O_4

View Article Online
DOI: 10.1039/C6NR00860G

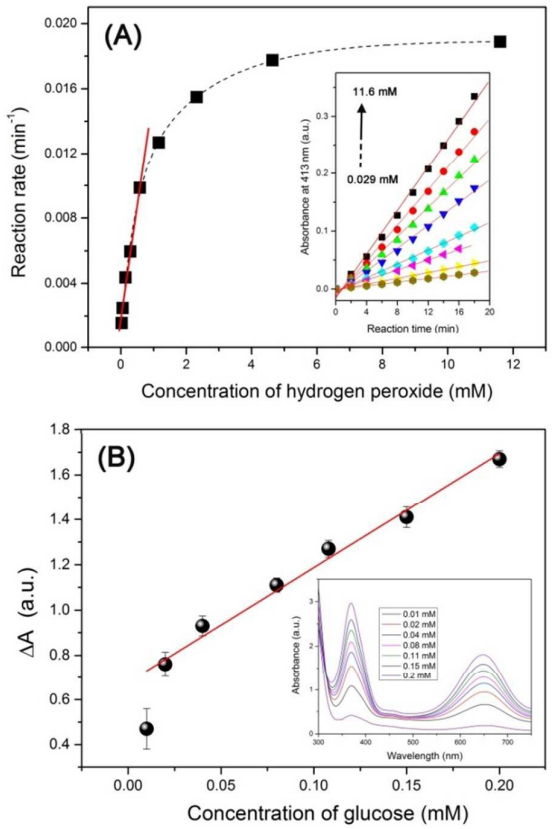

Figure 4 Concentration response for H_2O_2 (A) and glucose (B) detection using Co_3O_4 NPs as peroxidase mimic. Inset in (A) shows the absorbance evolution over reaction time at different H_2O_2 concentrations for OPD oxidation. Inset in (B) shows the evolution of the absorption with increasing glucose concentration.

As expected for the peroxidase-like activity of Co_3O_4 NPs, the initial reaction rates for both TMB and OPD oxidation were found to be strongly dependent on the concentration of H_2O_2 (**Figure 4A** and Figure S3). Hydrogen peroxide initiates the catalytic oxidation of TMB or OPD by Co_3O_4, and no evident oxidation was observed without H_2O_2. We observed that OPD and TMB oxidation reactions in the presence of Co_3O_4 NPs were accelerated with increasing H_2O_2 concentration. At lower concentrations of H_2O_2, a linear relationship between the reaction rate and H_2O_2 concentration was found. This linear response was the basis for the measurement of hydrogen peroxide concentration. For detection of H_2O_2 in the OPD oxidation reaction, the limit of detection for H_2O_2 is 0.015 mM, with linearity observed from 0.029 mM to 0.58 mM.

H_2O_2 is an important by-product involved in many biochemical reactions, such as the oxidation of glucose, uric acid, xanthine, and cholesterol. Thus, the concentrations of these biological molecules can be determined indirectly by detection of H_2O_2. For instance, glucose oxidase catalyzes the oxidation of glucose under oxygen-rich biological conditions to produce hydrogen peroxide and gluconic acid. Therefore, by combining the peroxidase-like activity of Co_3O_4 and the specific catalytic activity of glucose oxidase toward glucose, it is feasible to selectively detect glucose. **Figure 4B** shows the absorption evolution and absorbance change at 650 nm when the concentration of glucose increases. We observed that a higher concentration of glucose resulted in a higher absorption at 370 nm and 650 nm. The absorbance change at 650 nm was used to construct a standard curve of absorbance versus glucose concentration. This curve showed a good linear relationship, with R^2=0.99 in the glucose concentration range of 0.02 mM to 0.2 mM. The lower limit of detection was calculated to be 0.005 mM (S/N=3). Due to the high sensitivity, strong selectivity, and wide linear range of our system, this technique is suitable for blood glucose detection, as the concentration of glucose in human serum is in the range of 3 mM to 40 mM.[40] These results suggest that Co_3O_4 NPs can serve as a peroxidase in the colorimetric detection of glucose. They may potentially be used to detect other H_2O_2-related biomolecules for clinical diagnosis and personal health care applications.

In order to test the selectivity of proposed method for detection of glucose, control experiments were taken using glucose analogues, such as galactose, fructose and maltose. The concentrations of galactose, fructose and maltose were 1.0 mM, 5 times as high as glucose (0.2 mM). The results demonstrated that the method has high specificity to detection of glucose (**Figure 5**). For testing the feasibility of the method in real samples, we further detected the glucose concentration in human blood serum. The serum samples were spiked with desirable amounts of glucose, and the concentration of glucose was determined by the standard addition method (inset in **Figure 5**). The concentration of glucose in original blood was calculated to be 3.48 mM, which was slight lower than the provided value of 3.81 mM by GOD based glucose monitoring system from hospital. These results indicated this method based on the peroxidase-like activity of Co_3O_4 NPs can be applied specifically to glucose detection in real sample.

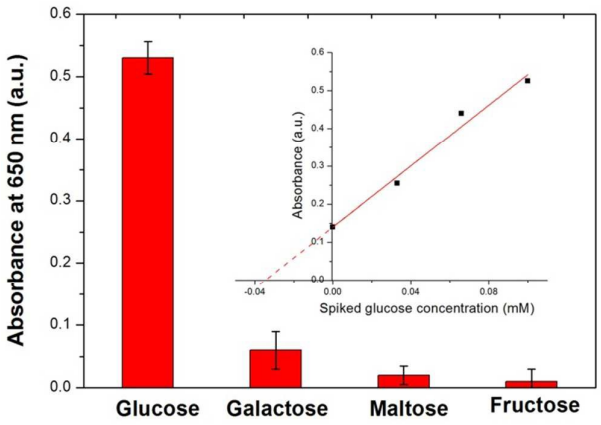

Figure 5 Selectivity of the proposed method for glucose detection. The concentrations were used as follow: 0.2 mM glucose, 1 mM galactose, 1 mM maltose and 1 mM fructose. The error bars represent the standard deviation of three measurements. Inset shows the standard addition method for detection of glucose in blood serum.

View Article Online
DOI: 10.1039/C6NR00860G

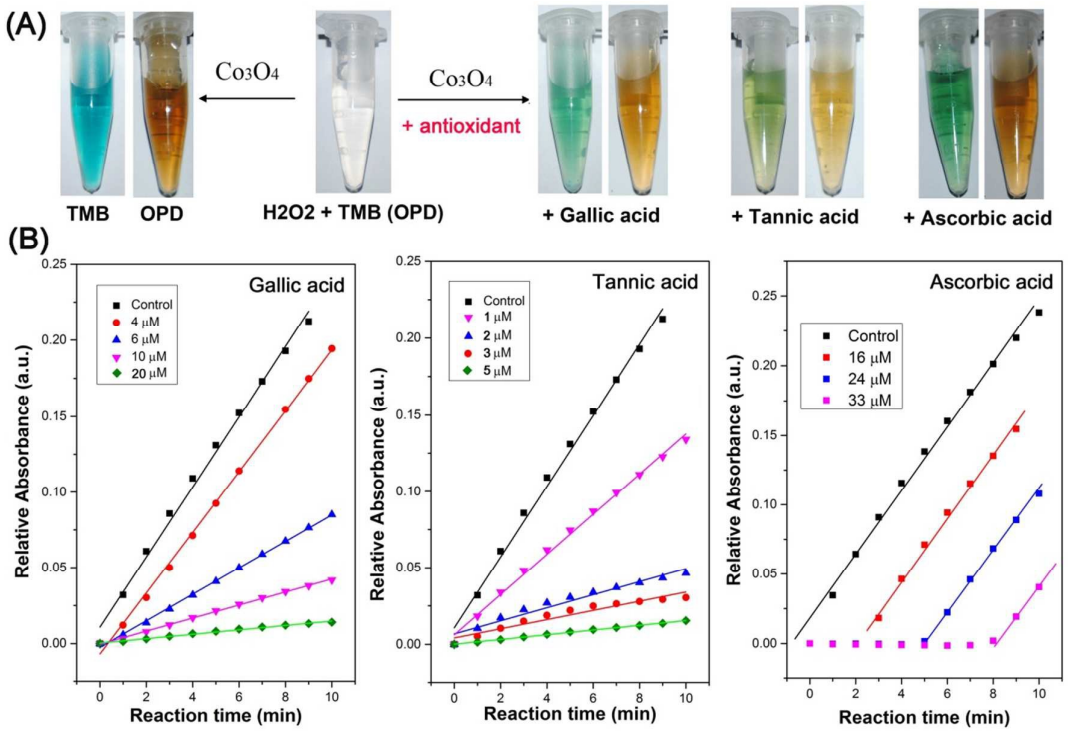

Figure 6. Quenching effect of gallic acid, tannic acid, and ascorbic acid on the peroxidase-like activity of Co_3O_4 NPs. (A) Photographs of typical chromogenic substrates after catalytic oxidation by Co_3O_4 NPs in the absence and presence of antioxidants GA (10μM), TA (5 μM) and AA (25 μM). (B) Concentration-dependent inhibition effects of GA, TA, and AA on the catalytic oxidation of TMB.

3.5. Inhibitory effect of antioxidants on the peroxidase-like activity of Co_3O_4 NPs

Gallic acid (GA), a type of phenolic acid, is found in gallnuts, sumac, tea leaves, and other plants, and is commonly used in the pharmaceutical industry to reduce the incidence of Alzheimer's disease and Parkinson's disease. Tannic acid (TA), a polymeric form of gallic acid, is a type of polyphenol widely used in the food industry and as medication for treatment of diverse diseases. Ascorbic acid (AA), a natural phytonutrient abundant in fruits and vegetables, is known to protect organisms against chronic diseases due to its antioxidant properties and has been widely used in foods, dietary supplements, and cosmetic products. We investigated the inhibitory effects of GA, TA, and AA on the peroxidase-like activity of Co_3O_4 NPs. Additionally, we used these three typical natural antioxidants to assess the practicality of our proposed method in evaluating antioxidant capacity. **Figure 6A** shows the color evolution of H_2O_2-mediated TMB and OPD oxidation reactions catalyzed by Co_3O_4 NPs. Addition of either gallic acid or tannic acid or AA reduced the oxidation rate of TMB and OPD compared with that of the antioxidant-free control reaction. TA was more efficient than GA in inhibiting the catalytic oxidation of TMB or OPD. The UV-vis spectral evolution of Co_3O_4-catalysed OPD oxidation over time in the absence and presence of GA is displayed in Figure S4. We also determined the quenching kinetics of the three antioxidants on the peroxidase-like activity of Co_3O_4 by recoding the absorbance of the TMB oxidation product over time (**Figure 6B**). From the slope of the Absorbance *vs* Reaction Time curve, we concluded that the oxidation rate of TMB was reduced with increasing concentrations of GA or TA, suggesting a concentration-dependent quenching effect. The three antioxidants show different levels of antioxidant activity in the following order: TA > GA > AA. TMB oxidation can be almost completely inhibited with 5 μM TA, compared to 20 μM GA or 30 μM AA. As shown in the chemical structures of the antioxidants (Figure S5), one tannic acid molecule is the polymeric product of ten gallic acid monomers. It is therefore reasonable that TA exhibits higher antioxidant efficiency than GA due to the presence of more phenolic groups in TA molecules.

Besides their different levels of antioxidant activity, the three antioxidants also exhibit different modes of inhibition. GA and TA exhibit similar trends, where the slope of the TMB oxidation plots decreased with increasing concentrations of GA or TA. Thus, the inhibition degree is linearly dependent on the concentration of GA or TA. In contrast, the plot slope at different concentrations of AA was unchanged, but the starting point of TMB oxidation was delayed proportionately to the concentration of AA. The delay time was linearly proportional to AA concentration. The inhibition modes of the three

View Article Online
DOI: 10.1039/C6NR00860G

antioxidants are illustrated in **Scheme 1**. GA and TA result in type I inhibition, while AA causes type II inhibition. The type I inhibition by GA or TA is dominated by two competitive reactions: the oxidation of the antioxidants vs. the oxidation of TMB by H_2O_2 under catalysis of Co_3O_4. The oxidation rate of TMB is thus decreased by increasing the antioxidant concentration. The type II inhibition caused by AA is due to a strong electron transfer occurring between AA and the catalyst surface, resulting in the reduction of active sites available for oxidation of TMB. When the AA is fully consumed, the oxidation of TMB starts. The initial reaction rate is then unaffected by the concentration of antioxidants. To prove the electron transfer occurring between AA and Co_3O_4 surface, we further monitored the reaction between AA and Co_3O_4 NPs (Figure S6). AA alone in the absence of Co_3O_4 NPs maintained good stability against oxidation by either soluble oxygen or 0.67 mM hydrogen peroxide. When AA mixed with Co_3O_4 NPs, the characteristic absorbance at 254 nm of AA decreased gradually with reaction time indicating the redox reaction happens between AA and Co_3O_4. As we discussed above, Co_3O_4 NPs with exposure of Co^{3+}/Co^{2+} species have the ability to oxidize AA (the reduction potential of AA is about -0.08 V).[41] As a result, Co^{3+} can get an electron from AA and turn into Co^{2+}, suggestive of the electron transfer reaction between Co_3O_4 and AA. For comparison, we have also monitored the reaction between GA (TA) and Co_3O_4 (Figure S6). The oxidations of both TA and GA by Co_3O_4 were negligible, indicating the weak electron transfer between TA or GA and Co_3O_4. However, the oxidation degree of TA and GA catalyzed by Co_3O_4 in the presence of H_2O_2 become obvious (Figure S6). These results indicated that inhibition effect of AA on peroxidase like activity is resulting from the electron transfer between Co_3O_4 and AA which affect the chemical surface of Co_3O_4 NPs, while the inhibition effect of TA and GA caused by their competitive reaction with hydrogen peroxide. These different mechanisms may indicate the distinctly inhibitory behavior among AA, TA and GA.

Our observations of different inhibition modes of antioxidants are consistent with previous reports on the inhibitory effects of Fe^{2+} and NaN_3 on the oxidase-like activity of Au@Pt nanostructures.[25] By using the peroxidase-like activity of Co_3O_4 NPs, we demonstrated that it is feasible to not only evaluate antioxidant activity and detect antioxidants, but also to identify the antioxidant behavior of various antioxidants and study their interactive mechanisms. It was expected that the antioxidant behavior of natural antioxidants for nanomaterials mimic can mirror to natural enzymes due to many reducing agents are enzyme inhibitors. This may provide a facile route to investigate the interaction between antioxidant inhibitors and natural enzymes. Many antioxidants are under investigation for their antioxidative activity and mechanism by using NP peroxidase mimics.

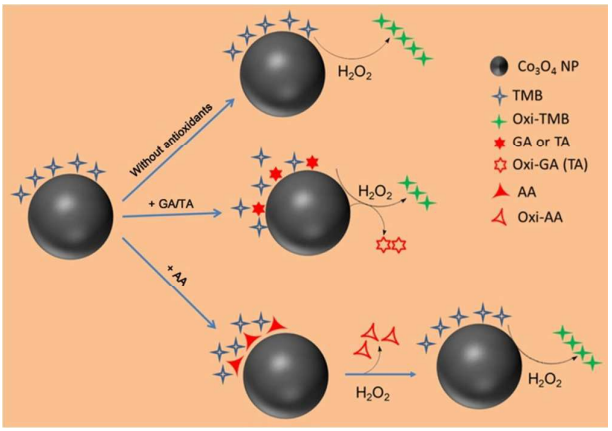

Scheme 1. Schematic illustration of different inhibition mechanisms in TMB oxidation catalyzed by Co_3O_4 NPs in the presence of H_2O_2: type I inhibition by GA or TA and type II inhibition by AA.

4. Conclusions

In this study, we employed the peroxidase-like activity of Co_3O_4 NPs to develop an effective platform for the detection of hydrogen peroxide and glucose. By studying the interaction of the Co_3O_4 NPs with antioxidants, we also evaluated the antioxidant activities of GA, TA, and AA. In terms of their ability to inhibit the artificial peroxidase-catalyzed oxidation of TMB or OPD, TA exhibits the highest antioxidant activity, followed by GA and AA. Interestingly, we found that the different antioxidants exhibited different modes of inhibition on peroxidase-like activity, with GA and TA showing type I inhibition and AA showing type II inhibition. This method is therefore an effective approach to evaluate antioxidants for their antioxidant capability or antioxidative mechanism. Since many antioxidants can inhibit the activity of natural enzymes, our results will also facilitate the investigation of biochemical interactions between enzymes and their inhibitors.

Acknowledgements

This work was supported by the National Natural Science Foundation of China (Grant No. 21303153 and 61204009), the Program for Science & Technology Innovation Talents in the Universities of Henan Province (14HASTIT008), and the Research Project of Higher Education and Teaching Reform of Henan Province (2014SJGLX064). We thank Prof. Jing Li and Yuejin An from Xinhua Hospital of Xuchang for their assistances with blood glucose analysis.

References

1 W. W. He, W. Wamer, Q. Xia, J.-J. Yin and P. P. Fu, *Journal of Environmental Science and Health, Part C*, 2014, **32**, 186-211.
2 H. Wei and E. Wang, *Chem. Soc. Rev.*, 2013, **42**, 6060–6093.
3 L. Gao, J. Zhuang, L. Nie, J. Zhang, Y. Zhuang, N. Gu, et al. *Nat. Nanotech.*, 2007, **2**, 577-583.
4 J. Dong, L. Song, J. Yin, W. He, Y. Wu, N. Gu and Y. Zhang, *ACS Appl. Mater. Interfaces*, 2014, **6**, 1959-1970.

View Article Online
DOI: 10.1039/C6NR00860G

5 A. Asati, S. Santra, C. Kaittanis, S. Nath and J. M. Perez, *Angew. Chem. Int. Ed.,* 2009, **48**, 2308 –2312.
6 R. André, F. Natálio, M. Humanes, J. Leppin, K. Heinze, R. Wever, H. C. Schröder, W. Müller, W. Tremel, *Adv. Funct. Mater.,* 2011, **21**, 501–509.
7 W. Chen, J. Chen, A. Liu, L.M. Wang, G. W. Li and X. H. Lin, *ChemCatChem*, 2011, **3**, 1151 – 1154.
8 X. Liu, Q. Wang, H. Zhao, L. Zhang, Y. Su and Y. Lv, *Analyst*, 2012, **137**, 4552.
9 W. W. He, H. Jia, X. Li, Y. Lei, J. Li, H. Zhao, L. Mi, L. Zhang and Z. Zheng, *Nanoscale*, 2012, 4, 3501;
10 A. K. Dutta, S. K. Maji, D. N. Srivastava, A. Mondal, P. Biswas, P. Paul and B. Adhikary, *ACS Appl. Mater. Interfaces,* 2012, 4, 1919−1927.
11 Y. Jv, B. Li, R. Cao, *Chem. Commun.*, 2010, 46, 8017–8019.
12 W. He, Y. Liu, J. Yuan, J. Yin, X. Wu, X. Hu, K. Zhang, J. Liu, C. Chen, Y. Ji and Y. Guo, *Biomaterials*, 2011, **32**, 1139–1147.
13 W. He, X. Wu, J. Liu, X. Hu, K. Zhang, S. Hou, W. Zhou and S. Xie, *Chem. Mater.,* 2010, **22**, 2988–2944.
14 X. Xia, J. Zhang, N. Lu, M. J. Kim, K. Ghale, Y. Xu, E. McKenzie, J. Liu and H. Ye, *ACS Nano*, 2015, **9**, 9994-10004.
15 J. Wei, X. Chen, S. Shi, S. Mo and N. Zheng, *Nanoscale*, 2015, DOI: 10.1039/C5NR05675F.
16 J. Yin, F. Lao, P. Fu, W. G. Wamer, Y. Zhao, P. C. Wang, Y. Qiu, B. Sun, G. Xing, J. Dong, X. Liang and C. Chen, *Biomaterials*, 2009, **30**, 611–621.
17 Y. Song, K. Qu, C. Zhao, J. Ren and X. Qu, *Adv. Mater.*, 2010, **22**, 2206–2210.
18 J. Zhang, H. Zhang, Z. Du, X. Wang, S. Yu and H. Jiang, *Chem. Commun.*, **2014**, 50, 1092
19 S. Li, H. Li, F. Chen, J. Liu, H. Zhang, Z. Yang and B. Wang, *Dyes and Pigments*, 2016, **125**, 64-71.
20 H. Sun, X. Jiao, Y. Han, Z. Jiang and D. Chen, *Eur. J. Inorg. Chem.*, 2013, 109–114
21 E. A. Veal, A. M. Day and B. A. Morgan, *Mol. Cell*, 2007, **26**, 1–14.
22 J. Liu, X. Hu, S. Hou, T. Wen, W. Liu, X. Zhu, J.-J. Yin and X. C. Wu, *Sensors and Actuators B*, 2012, **166– 167**, 708– 714.
23 X. X. Wang, Q. Wu, Z. Shan and Q. M. Huang, *Biosensors and Bioelectronics*, 2011, **26**, 3614–3619.
24 R. Zhu, Y. Zhou, X. Wang, L. Liang, Y. Long, Q. Wang, H. Zhang, X. Huang and H. Zheng, *Talanta*, 2013, **117**, 127–132.
25 J. Liu, X. Hu, S. Hou, T. Wen, W. Liu, X. Zhu and X. C. Wu, *Chem. Commun.*, 2011, **47**, 10981–10983
26 L. Li, L. Ai, C. Zhang and J. Jiang, *Nanoscale*, 2014, **6**, 4627.
27 Z. Zhang, J. Hao, W. Yang, B. Lu, X. Ke, B. Zhang and J. Tang, *ACS Appl. Mater. Interfaces*, 2013, **5**, 3809−3815.
28 H. Sies, *Experimental Physiology*, 1997, **82**, 291–5.
29 A. Ogawa, H. Arai, H. Tanizawa, T. Miyahara and Toshimasa Toyóoka, *Anal. Chim. Acta*, 1999, **383**, 221-230.
30 G. Cao, H. M. Alessio, R. G. Cutler, *Free Radic. Biol. Med.,* 1993, 14, 303–311.
31 A. J. Blasco, A. G. Crevillén, M. C. González and A. Escarpa, *Electroanalysis*, 2007, **19**, 2275-2286.
32 L. Wang, W. Ma, S. Gan, D. Han, Q. Zhang and L. Niu, *Anal. Chem.*, 2014, **86**, 10171−10178.
33 W. Yang, J. Hao, Z. Zhang, B. Zhang, *New J. Chem.*, 2015, **39**, 8802.
34 D. Vilela, M. C. González, A. Escarpa, *Trends in Analytical Chemistry*, 2015, **64**, 1–16.
35 E. Sharpe, S. Andreescu, *J. Chem. Educ.*, 2015, **92**, 886−891.
36 Y. Liu, H. H. Wu, Y. Chong, W. G. Wamer, Q. S. Xia, L.N. Cai, Z.H. Nie, P. P. Fu and J. J. Yin, *ACS Appl. Mater. Interfaces*, 2015, **7**, 19709−19717.
37 Y.-T. Zhou, W. He, W. G. Wamer, X. Hu, X. Wu, Y. M. Lo and J. Yin, *Nanoscale*, 2013, **5**, 1583.
38 X. Q. Zhang, S.W. Gong, Y. Zhang, T. Yang, C.-Y. Wang and N. Gu, *J. Mater. Chem.*, 2010, **20**, 5110–5116.
39 V. R. Mate, M. Shirai, C. V. Rode, *Catal. Commun.*, 2013, **33**, 66–69.
40 R. Badugu, J. R. Lakowicz and C. D. Geddes, *Anal. Chem.*, 2004, **76**, 610.
41 J. S. Fruton, *J. Biol. Chem.*, 1934, **105**, 79-85.